Energy Efficiency Optimization for CR-Enabled Integrated Terrestrial and NTNs with BD-RIS

(Invited Paper)

Wali Ullah Khan[†], Chandan Kumar Sheemar[†], Syed Tariq Shah[‡], Symeon Chatzinotas[†]
[†]Interdisciplinary Centre for Security, Reliability and Trust (SnT), University of Luxembourg, Luxembourg
{waliullah.khan, chandankumar.sheemar, symeon.chatzinotas}@uni.lu
[‡]School of Computer Science and Electronic Engineering, University of Essex, UK (syed.shah@essex.ac.uk)

***Abstract*—This paper presents a novel framework for cognitive radio (CR)-enabled integrated terrestrial and non-terrestrial networks (ITNTNs), comprising a primary low-Earth-orbit (LEO) satellite network and a secondary terrestrial network. In particular, a beyond-diagonal reconfigurable intelligent surface (BD-RIS) mounted secondary base station (BS) reuses the same spectrum to communicate with the secondary user. The proposed framework improves the energy efficiency of the secondary network while ensuring that the interference temperature threshold of the primary LEO network is not violated. The joint optimization of BS power allocation and BD-RIS phase shifts is considered, which results in a highly nonconvex problem. To address this challenge, the Dinkelbach method is first employed to transform the fractional objective function, followed by the development of an alternating optimization strategy. Specifically, the BS power allocation is optimized using the Lagrangian method with Karush-Kuhn-Tucker (KKT) conditions, while the BD-RIS phase shifts are updated through manifold optimization techniques. Numerical results demonstrate that the proposed BD-RIS framework performs better than conventional diagonal RIS (D-RIS) configurations in terms of energy and spectral efficiency, highlighting its potential to enable green, adaptive, and high-capacity 6G ITNTN deployments.**

***Index Terms*—Beyond diagonal RIS, CR network, integrated terrestrial NTNs, energy and spectral efficiency.**

I. Introduction

The evolution toward sixth-generation (6G) networks envisions a deeply integrated terrestrial and non-terrestrial (ITNTN) ecosystem, comprising ground base stations (BSs), drones, high-altitude platform stations (HAPS), and satellites, to achieve ubiquitous connectivity across the globe [1]. This seamless convergence promises ultra-low latency, massive IoT scalability, and reliable coverage even in remote areas [2]. By harmonizing ITNTNs, 6G aims to deliver unprecedented data rates, global service continuity, and robust support for critical applications such as remote healthcare, autonomous transportation, and smart cities [3], [4]. However, realizing this vision requires overcoming challenges such as dynamic spectrum co-existence, interference management in hybrid networks, and energy-efficient resource allocation across heterogeneous nodes [5].

Beyond diagonal reconfigurable intelligent surfaces (BD-RIS) and cognitive radio (CR) are emerging as key enablers for dynamic spectrum access and spectral efficient 6G networks [6], [7]. CR improves spectral agility by intelligently exploiting underutilized radio frequency (RF) bands among multilayer ITNTNs, while BD-RIS extends traditional diagonal RIS (D-RIS) capabilities with advanced beamforming and interference mitigation [8], [9]. Together, they promise significant improvements in spectral efficiency, coverage extension, and adaptive resource utilization for ITNTNs [10]. However, maximizing energy efficiency in such systems requires overcoming key challenges, including power-constrained reconfigurability, trade-offs between spectral and energy performance, and dynamic resource allocation under varying channel conditions. Addressing these optimization issues is essential for realizing green, high-capacity 6G ITNTNs with minimal carbon footprint.

Most existing studies on BD-RIS have primarily focused on terrestrial wireless networks. For example, works such as [11], [12] addressed channel estimation techniques in BD-RIS-assisted multiple-input multiple output (MIMO) systems. Other studies [7], [13], [14] explored the use of BD-RIS to enhance metrics like achievable rate, spectral efficiency, and energy efficiency. In addition, [15], [16] examined how BD-RIS can benefit integrated sensing and communication (ISAC) in 6G wireless networks. Furthermore, BD-RIS has also been applied in terahertz (THz) communication to improve coverage in various environments, as discussed in [17], [18].

More recently, the use of BD-RIS in NTNs has gained research interest. For example, [1] employed BD-RIS to support LEO satellite communications, focusing on joint transmit power and RIS response optimization to enhance the sum rate of the system. Similarly, [19] proposed a multi-user multi-carrier communication system assisted by

drones using transmissive BD-RIS, where power allocation and beamforming were jointly optimized to improve user's data rates. In another related work, [20] investigated a LEO-based transmissive BD-RIS setup for IoT connectivity, with the aim of maximizing the sum rate through coordinated resource allocation. Despite these advancements, the exploration of BD-RIS in ITNTNs remains limited and needs further investigation.

This work introduces a novel framework for CR-enabled ITNTNs, comprising a primary LEO satellite system and a secondary terrestrial BS equipped with a transmissive BD-RIS. The objective is to enhance the spectral and energy efficiency of the terrestrial network through transmit power and phase response optimization while ensuring that the interference to the primary LEO system remains within acceptable limits. The joint energy efficiency optimization is nonconvex, which poses a high complexity. To efficiently tackle this, we first exploit a Dinkelbach method to reduce the overall complexity of the joint problem, and then adopt an alternating optimization method, where the problem is divided into two subproblems and solved iteratively. Given the transmissive phase response of BD-RIS, the transmit power is optimized for BS using the Lagrangian method with Karush-Kuhn-Tucker (KKT) conditions. Then, the phase shift for BD-RIS is designed via manifold optimization, given the transmit power of BS. The numerical results are provided to validate and compare the proposed solution with the conventional D-RIS configuration. The remainder of our work is structured as follows: the proposed scenario for ITNTN and the steps in formulating energy efficiency are described in Section II; Section III outlines the proposed energy-efficient approach; Section IV discusses the simulation results, and Section V concludes the this paper.

II. Proposed ITNTN Scenario and Energy Efficiency Formulation

We consider cognitive radio-enabled ITNTNs comprising primary and secondary networks. The primary network consists of an LEO transmitter that serves primary user equipment (PUE). At the same time, a terrestrial BS equipped with a transmissive BD-RIS constitutes a secondary network by using the same spectrum simultaneously and serves secondary user equipment (SUE). We assume that the SUE follows a single antenna and BD-RIS comprises M reconfigurable elements with fully-connected architecture. The system architecture is illustrated in Fig.1.We aim to improve the energy and spectral efficiency of terrestrial network through joint BS's power and BD-RIS phase-response optimization, subject to the interference temperature constraint from a secondary BS to PUE. The vector of the wireless channel $\mathbf{h} \in \mathbb{C}^{M\times 1}$ from BS to SUE is modeled as a Rayleigh fading channel, which captures the effects of multipath propagation

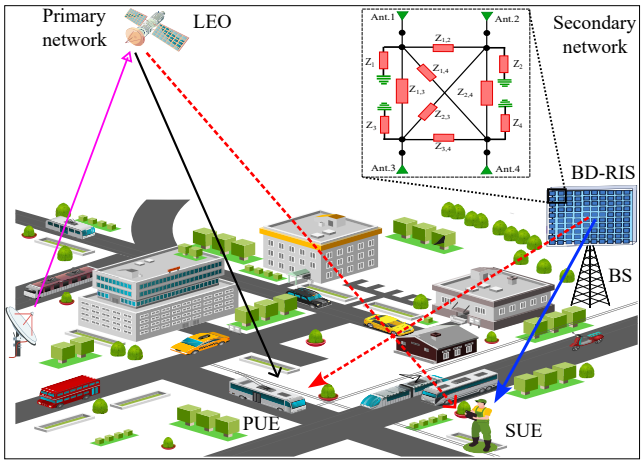

Fig. 1: System model.

in the absence of a dominant line-of-sight (LoS) component. The channel vector can be expressed as:

$$\mathbf{h} = \sqrt{\frac{\hat{h}}{d_h^{\alpha}}}\,\mathbf{h}_{\text{NLoS}}, \quad \mathbf{h}_{\text{NLoS}} \sim \mathcal{CN}(\mathbf{0}, \mathbf{I}_M), \tag{1}$$

where $\hat{h}$ denotes the reference channel power gain at a unit distance, d_f is the distance between the BS and the SUE, and α is the path-loss exponent, typically ranging from 2 to 4 depending on the propagation environment. The vector $\mathbf{h}_{\text{NLoS}}$ represents small-scale fading and follows a circularly symmetric complex Gaussian distribution, denoted as $\mathcal{CN}(\mathbf{0}, \mathbf{I}_M)$, where the elements are independent and identically distributed (i.i.d.) complex Gaussian random variables with zero mean and unit variance. This statistical model is widely adopted for urban or indoor environments characterized by rich scattering and no dominant LoS path. Similarly, the channels from the BS to the PUE and from the LEO to the SUE are denoted as $\mathbf{g} \in \mathbb{C}^{M\times 1}$ and $f \in \mathbb{C}^{1\times 1}$, respectively, and are modelled as Rayleigh fading[1] which can be described as:

$$\mathbf{g} = \sqrt{\frac{\hat{g}}{d_g^{\alpha}}}\,\mathbf{g}_{\text{NLoS}}, \quad \mathbf{g}_{\text{NLoS}} \sim \mathcal{CN}(0, \mathbf{I}_M), \tag{2}$$

$$f = \sqrt{\frac{\hat{f}}{d_f^{\alpha}}}\,f_{\text{NLoS}}, \quad f_{\text{NLoS}} \sim \mathcal{CN}(0, 1). \tag{3}$$

where $\hat{g}$ and $\hat{f}$ are the power gains of the reference channel at a unit distance, d_g and d_f denote the distance between the BS and the PUE and between the LEO and the SUE.

[1]While the LEO-to-ground channel typically exhibits Rician fading due to the presence of a strong LoS component, we adopt a Rayleigh fading model under the assumption of a dense urban environment, where buildings and other structures often obstruct the LoS path.

Additionally, α is the path loss exponent, which ranges from 2 to 4, depending on the propagation environment. The received signal at SUE from BS can be expressed as:

$$y = \mathbf{h}\boldsymbol{\Theta}\sqrt{P_s}x + f\sqrt{Q_p}z + n_s, \tag{4}$$

where x and z are independent and identically distributed (i.i.d.) unit-variance data streams of BS and LEO satellite, respectively. The matrix $\boldsymbol{\Theta} \in \mathbb{C}^{M_x \times M_y}$ represents the phase response matrix of transmissive BD-RIS, satisfying the unitary constraint as $\boldsymbol{\Theta}\boldsymbol{\Theta}^H = \mathbf{I}_M$. Here, M_x and M_y are the total phase response elements in the x-axis and y-axis, respectively. The term $n_s \sim \mathcal{CN}(0, \sigma^2)$ represents additive white Gaussian noise (AWGN) with variance σ^2, while P_s and Q_p denote the powers of BS and LEO satellite, respectively. The achievable rate at the SUE can be calculated as:

$$R_s = \log_2(1 + \eta_s), \tag{5}$$

where η_s denotes the signal-to-interference-plus-noise ratio (SINR), defined as:

$$\eta_s = \frac{|\mathbf{h}\boldsymbol{\Theta}|^2 P_s}{\sigma^2 + |f|^2 Q_p}. \tag{6}$$

To guarantee the communication quality of the primary network, the interference power received in the PUE signal is bounded by an interference temperature threshold I_{th}, and must satisfy the following condition:

$$|\mathbf{g}\boldsymbol{\Theta}|^2 P_s \leq I_{\text{th}}. \tag{7}$$

This work aims to improve the achievable energy efficiency of the terrestrial network, defined as the ratio of the achievable rate to the total power consumption. The optimization problem can be formulated as follows.

$$\mathcal{P}: \quad \max_{P_s, \boldsymbol{\Theta}} \quad \frac{R_s}{P_s + P_c} \tag{8}$$

$$\text{s.t.} \quad C_1: |\mathbf{g}\boldsymbol{\Theta}|^2 P_s \leq I_{\text{th}}, \tag{9}$$

$$C_2: 0 \leq P_s \leq P_{tot}, \tag{10}$$

$$C_3: \boldsymbol{\Theta}\boldsymbol{\Theta}^H = \mathbf{I}_M, \tag{11}$$

where $P_c = p_{\text{BS},c} + p_{\text{RIS},c} + p_{\text{RIS-BD}}$ represents the total circuit power consumption (CPC) of the system. Specifically, $p_{\text{BS},c}$ denotes the CPC of the BS, and $p_{\text{RIS},c}$ refers to the controller power consumption of the fully-connected BD-RIS. Moreover, the term $p_{\text{RIS-BD}}$ accounts for the power consumption of the fully-connected impedance network in the BD-RIS. Based on graph theory, the number of edges in a fully-connected undirected graph with M elements is $M(M-1)/2$ [21]. Therefore, the impedance network power consumption can be expressed as:

$$p_{\text{RIS-BD}} = \left(M + \frac{M(M-1)}{2}\right) \cdot p_e, \tag{12}$$

where p_e denotes the power consumption per impedance connection between two BD-RIS elements. In (10), P_{tot} is the total transmit power of BS. Furthermore, constraint C_1 ensures the interference temperature at the PUE remains below the threshold I_{th}, C_2 controls the transmission of terrestrial BS, and C_3 enforces the unitary constraint on the phase response matrix of BD-RIS. This optimization problem is nonconvex due to the coupling between P_s and $\boldsymbol{\Theta}$. Moreover, the objective function in optimization problems is typically a ratio of achievable rate to power consumption, which leads to fractional programming. The lack of prior work on similar problems necessitates the development of novel algorithmic solutions tailored to this scenario.

III. Proposed Energy Efficient Solution

The original objective function is fractional (ratio of two functions), which is difficult to solve directly because it is neither concave nor convex. To address this, we adopt the Dinkelbach method, which efficiently converts the ratio in the objective function into a subtractive form. Let us introduce an auxiliary variable λ and transform the objective function of energy efficiency as:

$$\max_{P_s, \boldsymbol{\Theta}} \; R_s - \lambda(P_s + P_c). \tag{13}$$

where λ is a scalar parameter that represents the energy efficiency (in bits per Joule) achieved at each iteration. At convergence, λ equals the optimal energy efficiency of the system and can be expressed as:

$$\lambda^* = \frac{R_s^*}{P_s^* + P_c}. \tag{14}$$

where R_s^* and P_s^* are the optimal rate and power, respectively. By incorporating this, the energy efficiency optimization in problem $\mathcal{P}$ can be revised as:

$$\mathcal{P}_1: \quad \max_{P_s, \boldsymbol{\Theta}} \; R_s - \lambda(P_s + P_c) \tag{15}$$

$$\text{s.t.} \quad C_1: |\mathbf{g}\boldsymbol{\Theta}|^2 P_s \leq I_{\text{th}}, \tag{16}$$

$$C_2: 0 \leq P_s \leq P_{tot}, \tag{17}$$

$$C_3: \boldsymbol{\Theta}\boldsymbol{\Theta}^H = \mathbf{I}_M, \tag{18}$$

It can be observed that the optimization variables in $\mathcal{P}_1$ are coupled, resulting in nonconvex optimization. In addition, the interference term in the rate expression and the unitary constraint make the optimization complex. Thus, $\mathcal{P}_1$ is first decoupled into two subproblems, and then alternating optimization is employed to get an efficient solution. For

a given $\mathbf{\Theta}$, the problem $\mathcal{P}_1$ reduces to a power allocation problem as follows:

$$\mathcal{P}_{1.1}: \quad \max_{P_s} \; R_s - \lambda(P_s + P_c) \tag{19}$$

$$\text{s.t.} \quad C_1 : |\mathbf{g\Theta}|^2 P_s \leq I_{\text{th}}, \tag{20}$$

$$C_2 : 0 \leq P_s \leq P_{tot}, \tag{21}$$

Now, we use the Lagrangian method and define the Lagrangian function of $\mathcal{P}_{1.1}$ as:

$$\mathcal{L}(P_s, \mu, \delta) = \log_2(1+\gamma_s) - \lambda P_s + \mu(I_{\text{th}} - |\mathbf{g\Theta}|^2 P_s) + \delta(P_{tot} - P_s). \tag{22}$$

where μ and δ are the Lagrangian multipliers. The optimal power is derived from the KKT conditions by deriving (22) with respect to P_s and setting it equal to zero to obtain the optimal power P_s^* as:

$$\frac{\partial \mathcal{L}(P_s, \mu, \delta)}{\partial P_s} = \frac{\partial}{\partial P_s}(\log_2(1+\gamma_s) - \lambda P_s + \mu(I_{\text{th}} - |\mathbf{g\Theta}|^2 P_s) + \delta(P_{tot} - P_s)) = 0. \tag{23}$$

Solving for P_s, it can be expressed as:

$$P_s = \frac{1}{(\lambda + \mu|\mathbf{g\Theta}|^2 + \delta).\ln(2)} - \frac{\sigma^2 + |f|^2 Q_p}{|\mathbf{h\Theta}|^2}. \tag{24}$$

Detailed derivations can be found in Appendix A. Note that the value of P_s must satisfy the transmit power constraint and the interference temperature constraint. If the calculated P_s violates these constraints, it must be projected back into the feasible region as:

- If $P_s < 0$, set $P_s = 0$.
- If $P_s > P_{tot}$, set $P_S = P_{tot}$.
- If $|\mathbf{g\Theta}|^2 P_s > I_{\text{th}}$, set $P_s = I_{\text{th}}/|\mathbf{g\Theta}|^2$.

Based on these conditions, the optimal power P_s^* can be described as:

$$P_s^* = \max\left(0, \min\left(P_{tot}, \frac{1}{(\lambda + \mu|\mathbf{g\Theta}|^2 + \delta).\ln(2)} - \frac{\sigma^2 + |f|^2 Q_p}{|\mathbf{h\Theta}|^2}, \frac{I_{\text{th}}}{|\mathbf{g\Theta}|^2}\right)\right) \tag{25}$$

Next, we update the Lagrangian multipliers using the subgradient method as:

$$\mu^{k+1} = \mu^k + \alpha^k(|\mathbf{g\Theta}^k|^2 P_s^k - I_{\text{th}}). \tag{26}$$

$$\delta^{k+1} = \delta^k + \alpha^k(P_s^k - P_{tot}). \tag{27}$$

where α is the non-zero step size and k shows the iteration index. In each iteration k, we compute P_s and update μ and δ until convergence.

Given the transmit power of BS P_s, the energy efficiency optimization can be simplified to a BD-RIS phase shift design problem such as:

$$\mathcal{P}_{1.2}: \quad \max_{\mathbf{\Theta}} \; \log_2(1+\eta_s) - \lambda(P_s + P_c) \tag{28}$$

$$\text{s.t.} \quad C_1 : |\mathbf{g\Theta}|^2 P_s \leq I_{\text{th}}, \tag{29}$$

$$C_3 : \mathbf{\Theta\Theta}^H = \mathbf{I}_M, \tag{30}$$

We can see that the problem $\mathcal{P}_{1.2}$ is still nonconvex due to the interference term in the rate expression and the unitary constraint on the BD-RIS phase shift. Thus, solving this problem is challenging and requires a powerful optimization approach. This motivates us to adopt manifold optimization, which is an effective method to handle unitary-constrained optimization problems. In this approach, $\mathbf{\Theta}$ is considered as a point on the Stiefel manifold, which comprises all $M \times M$ unitary matrices. The Stiefel manifold $St(M, M)$ is formally defined as:

$$St(M, M) = \{\mathbf{\Theta} \in \mathcal{C}^{M \times M} | \mathbf{\Theta\Theta}^H = \mathbf{I}_m\}. \tag{31}$$

Next, we describe a Lagrangian function corresponding to optimization $\mathcal{P}_{1.2}$ such as:

$$\mathcal{L}(\mathbf{\Phi}, \lambda) = \log_2\left(1 + \frac{|\mathbf{h\Theta}|^2 P_s}{\sigma^2 + |f|^2 Q_p}\right) - \mu(P_s + P_c) - \lambda(|\mathbf{g\Phi}|^2 P_s - I_{\text{th}}) \tag{32}$$

where μ and λ denote the Lagrange multipliers. The Euclidean gradient of the objective function with respect to $\mathbf{\Theta}$ is given by:

$$\nabla_{\mathbf{\Theta}} \mathcal{L}(\Theta, \mu, \lambda) = \frac{2P_s}{\ln(2)}\left(\frac{\mathbf{h}_s^H \mathbf{h}_s \mathbf{\Theta}}{(1+\gamma_s)(\sigma^2 + |f_s|^2 Q_p)}\right) - 2\lambda P_s(\mathbf{g}^H \mathbf{\Theta})\mathbf{g}. \tag{33}$$

The derivation of (33) is provided in Appendix A. While the Euclidean gradient gives the steepest ascent direction in Euclidean space, it does not satisfy the manifold's constraints. Therefore, it must be projected onto the tangent space of the Stiefel manifold at the current point Θ^k, where k denotes the iteration index. The projection is computed as:

$$\text{grad}_{\mathbf{\Theta}} \mathcal{L} = \nabla_{\mathbf{\Theta}} \mathcal{L} - \mathbf{\Theta}^k (\nabla_{\mathbf{\Theta}} \mathcal{L})^H \mathbf{\Theta}^k, \tag{34}$$

We update Θ on the Stiefel manifold using the matrix exponential method as:

$$\Theta^{k+1} = \Theta^i \text{Exp}(\beta^k . \text{grad}_{\Theta} \mathcal{L}) \tag{35}$$

where β represents the step size. If the interference threshold I_{th} is violated in any iteration, the update is projected back to the feasible region by adjusting β^k as:

$$\beta^k = \min\left(\beta^k, \frac{I_{\text{th}}}{|\mathbf{g\Theta}|^2 P_s}\right). \tag{36}$$

TABLE I: Simulation Parameters

Parameter	Value
Number of BD-RIS elements (M)	32, 64
Total transmit power of BS (P_{tot})	40 dBm
BS circuit power (p_c)	100 mW
Power per RIS element (p_e)	2 mW
RIS controller power ($p_{\text{ris,c}}$)	100 mW
BD-RIS total power (p_{risBD})	As per Eq. (12)
D-RIS total power (p_{risD})	$M \times p_e$
Interference temperature limit (I_{th})	-30 dBm
LEO satellite transmit power (Q_p)	40 dBm
Noise power variance (σ^2)	10^{-7}
Distance BS to SUE (d)	300 m
Distance BS to PUE (d_g)	500 m
Distance LEO to SUE (d_f)	340,000 m

The tangent space acts as a local linear approximation of the manifold at $\boldsymbol{\Theta}^k$, and this projection ensures that updates remain within the geometric constraints of the manifold. This links the Euclidean gradient in (33) with the manifold structure defined in (32), ensuring compliance with the unitary constraint. This iterative process continues, refining $\boldsymbol{\Theta}$ until convergence. The step size β_i controls progression along the manifold's geodesic path, ensuring stability and efficiency.

The per-iteration complexity is dominated by matrix operations, with an order of $\mathcal{O}(M^3)$ for an $M \times M$ RIS.

IV. Results and Discussion

This section provided the numerical results based on Monte Carlo simulation (1000 realizations). The results are provided for the proposed CR-enabled ITNTNs using D-RIS and BD-RIS configurations. Unless mentioned the simulation parameters are described in Table I.

Fig. 2 illustrates the achievable energy efficiency (AEE) performance of BD-RIS and D-RIS architectures versus their energy consumption P_{ris}, for two different values of RIS elements, $M = 32$ and $M = 64$. It can be observed that the system with fewer BD-RIS elements achieves higher AEE compared to the case with a larger number of elements. This is because BD-RIS performs better when the number of elements is small due to fewer interconnection impedance and reduced signal processing overhead, resulting in lower energy consumption. Moreover, BD-RIS significantly outperforms D-RIS in terms of AEE when the per-element energy consumption is low. However, as the per-element power consumption increases, the energy efficiency of BD-RIS declines more rapidly, owing to the increased complexity of interconnections and associated power overhead. In contrast, D-RIS exhibits relatively stable but consistently lower AEE due to its simpler architecture. These findings highlight the trade-off between reconfigurability and energy efficiency in BD-RIS, especially under varying hardware complexity.

Fig. 3 presents the AEE performance of BD-RIS and D-RIS versus the transmit power of the secondary BS,

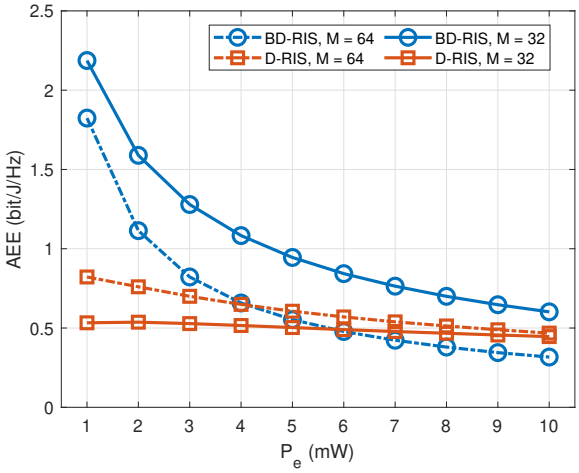

Fig. 2: Varying P_e versus system AEE.

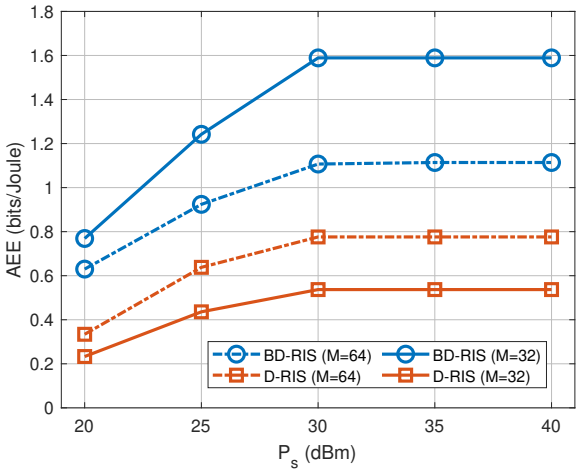

Fig. 3: Vaying BS power versus system AEE.

denoted by P_s, for two different values of RIS elements, $M = 32$ and $M = 64$. It is observed that the AEE initially increases with increasing P_s, but eventually saturates and remains constant beyond a certain transmit power threshold. This behaviour can be attributed to two potential reasons. First, the transmit power beyond the saturation point may cause the interference temperature constraint I_{th} at the primary network to be violated, which prevents the algorithm from allocating additional power. Second, it is possible that increasing P_s further leads to diminishing returns in terms of achievable rate, while increasing power consumption, thereby reducing AEE. To avoid a decline in energy efficiency, the algorithm restricts further power increments, even when higher power is available. Overall,

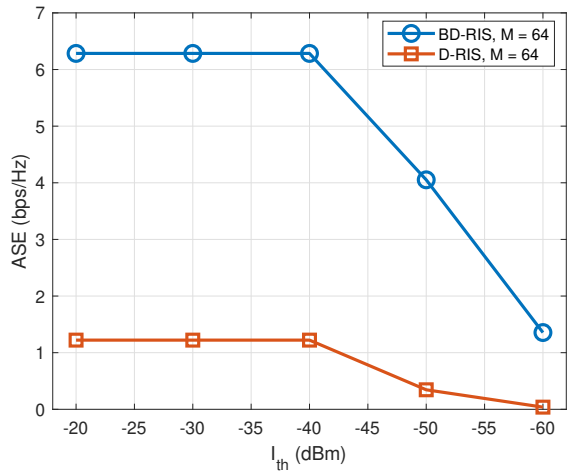

Fig. 4: Vaying interference threshold versus system ASE.

BD-RIS consistently achieves higher AEE than D-RIS for all P_s values, reaffirming its potential for energy-efficient communication under interference-limited scenarios.

We also investigated the achievable spectral efficiency (ASE) of the system against the varying interference threshold I_{th} from the secondary network to the primary network, as shown in Fig. 4. For this plot, we set $P_s = 40$ dBm and $\sigma^2 = 10$ μW. It is observed that BD-RIS achieves significantly higher ASE compared to D-RIS across all interference levels, highlighting its superior beamforming and signal-focusing capabilities. As I_{th} becomes more stringent (i.e., more negative), the ASE of both systems decreases. However, BD-RIS maintains a higher ASE over a broader range of I_{th} values, demonstrating its ability to better adapt to strict interference constraints. In contrast, the D-RIS exhibits relatively flat and low ASE, showing minimal adaptation to changes in I_{th} due to its limited reconfigurability. These results underscore the effectiveness of BD-RIS in maintaining high data rates even under tight interference constraints, making it a promising candidate for underlay spectrum-sharing scenarios in cognitive radio networks.

V. Conclusion

This work studied a CR-enabled ITNTN framework that employs a transmissive BD-RIS to maximize the energy efficiency of the secondary network under interference constraints from the primary LEO network. The joint optimization problem was solved using alternating optimization. Numerical results demonstrated that BD-RIS achieves higher AEE than D-RIS, particularly when the number of RIS elements is moderate and the per-element energy consumption is low. However, as hardware complexity and power overhead increase, the energy advantage of BD-RIS decreases. Furthermore, BD-RIS consistently outperforms D-RIS in terms of AEE across varying BS transmit powers, and it maintains superior ASE under stringent interference constraints. These findings highlight the trade-offs between energy efficiency, reconfigurability, and complexity in BD-RIS systems and underscore ITS potential as a key enabler for sustainable 6G ITNTN deployments.

Appendix A: Derivation of Equation (24)

To calculate the derivative of (24), we need to carefully differentiate each term with respect to P_s. Let's break it down step by step. The Lagrangian can be defined as:

$$\mathcal{L}(P_s,\mu,\delta) = \log_2\left(1+\frac{|\mathbf{h\Theta}|^2 P_s}{\sigma^2+|f|^2Q_p}\right) - \lambda P_s + \mu(I_{\text{th}} - |\mathbf{g\Theta}|^2 P_s) + \delta(P_{\text{tot}} - P_s), \quad (37)$$

Let $A = |\mathbf{h\Theta}|^2$ and $B = \sigma^2 + |f|^2 Q_p$. Then, the derivative with respect to P_s can be expressed as:

$$\frac{\partial}{\partial P_s}\log_2\left(1+\frac{AP_s}{B}\right) = \frac{1}{\ln(2)}\cdot\frac{1}{1+\frac{AP_s}{B}}\cdot\frac{A}{B}. \quad (38)$$

Simplifying (38) as:

$$\frac{\partial}{\partial P_s}\log_2\left(1+\frac{AP_s}{B}\right) = \frac{A}{\ln(2)(B+AP_s)}. \quad (39)$$

Next, we differentiate the remaining terms in the Lagrangian with respect to P_s as:

$$\frac{\partial}{\partial P_s}(-\lambda P_s + \mu(I_{\text{th}} - |\mathbf{g\Theta}|^2 P_s) + \delta(P_{\text{tot}} - P_s) = -\lambda - \mu|\mathbf{g\Theta}|^2 - \delta \quad (40)$$

Combining the derivatives of all terms such as:

$$\frac{\partial\mathcal{L}(.)}{\partial P_s} = \frac{A}{\ln(2)(B+AP_s)} - \lambda - \mu|\mathbf{g\Theta}|^2 - \delta. \quad (41)$$

To compute P_s, we ubstitute the values of A and B in and set the derivative of the Lagrangian $\mathcal{L}(P_s,\mu,\delta)$ with respect to P_s to zero as:

$$\frac{|\mathbf{h\Theta}|^2}{\ln(2)(\sigma^2+|f|^2Q_p+|\mathbf{h\Theta}|^2P_s)} = \lambda + \mu|\mathbf{g\Theta}|^2 + \delta. \quad (42)$$

Multiply both sides by the denominator on the left-hand side, and it can be written as:

$$|\mathbf{h\Theta}|^2 = (\lambda+\mu|\mathbf{g\Theta}|^2+\delta) \cdot \ln(2)(\sigma^2+|f|^2Q_p+|\mathbf{h\Theta}|^2P_s). \quad (43)$$

We first divide both sides by $(\lambda+\mu|\mathbf{g\Theta}|^2+\delta)\cdot\ln(2)$ and then subtract $\sigma^2+|f|^2Q_p$ from both sides; it is given as:

$$\frac{|\mathbf{h\Theta}|^2}{(\lambda+\mu|\mathbf{g\Theta}|^2+\delta)\cdot\ln(2)} - (\sigma^2+|f|^2Q_p) = |\mathbf{h\Theta}|^2P_s. \quad (44)$$

Finally, we divide both sides by $|\mathbf{h\Theta}|^2$ to solve for P_s, the expression for P_s can be simplified as:

$$P_s = \frac{1}{(\lambda + \mu|\mathbf{g\Theta}|^2 + \delta) \cdot \ln(2)} - \frac{\sigma^2 + |f|^2 Q_p}{|\mathbf{h\Theta}|^2}. \quad (45)$$

REFERENCES

[1] W. U. Khan, M. Ahmed *et al.*, "Survey on beyond diagonal ris enabled 6g wireless networks: Fundamentals, recent advances, and challenges," *arXiv preprint arXiv:2503.08423*, 2025.

[2] A. Hazra, A. Munusamy, M. Adhikari, L. K. Awasthi, and V. P, "6g-enabled ultra-reliable low latency communication for industry 5.0: Challenges and future directions," *IEEE Communications Standards Magazine*, vol. 8, no. 2, pp. 36–42, June 2024.

[3] C. K. Sheemar, P. Thiruvasagam *et al.*, "Joint communications and sensing for 6G satellite networks: Use cases and challenges," *arXiv preprint arXiv:2501.05243*, 2025.

[4] G. Iacovelli, C. K. Sheemar *et al.*, "Holographic MIMO for next generation non-terrestrial networks: Motivation, opportunities, and challenges," *arXiv preprint arXiv:2411.10014*, 2024.

[5] W. U. Khan, Z. Ali *et al.*, "Rate splitting multiple access for next generation cognitive radio enabled LEO satellite networks," *IEEE Trans. Wireless Commun.*, vol. 22, no. 11, pp. 8423–8435, 2023.

[6] Z. Ali, W. U. Khan *et al.*, "Enhanced learning-based hybrid optimization framework for RSMA-aided underlay LEO communication with non-collaborative terrestrial primary network," *IEEE Trans. Commun.*, pp. 1–1, 2024.

[7] C. Zhang, W. U. Khan *et al.*, "Sum rate maximization for 6g beyond diagonal RIS-assisted multi-cell transportation systems," *IEEE Transactions on Intelligent Transportation Systems*, pp. 1–11, 2025.

[8] M. Ahmed, S. Raza *et al.*, "Active reconfigurable intelligent surfaces: Expanding the frontiers of wireless communication-a survey," *IEEE Communications Surveys & Tutorials*, pp. 1–1, 2024.

[9] P. T. Tin, M.-S. V. Nguyen *et al.*, "Performance analysis of user pairing for active RIS-enabled cooperative NOMA in 6G cognitive radio networks," *IEEE Internet of Things Journal*, vol. 11, no. 23, pp. 37 675–37 692, Dec. 2024.

[10] S. Shen, B. Clerckx, and R. Murch, "Modeling and architecture design of reconfigurable intelligent surfaces using scattering parameter network analysis," *IEEE Transactions on Wireless Communications*, vol. 21, no. 2, pp. 1229–1243, 2022.

[11] H. Li, S. Shen *et al.*, "Channel estimation and beamforming for beyond diagonal reconfigurable intelligent surfaces," *IEEE Transactions on Signal Processing*, vol. 72, pp. 3318–3332, 2024.

[12] G. T. de Araujo and A. L. de Almeida, "Semi-blind channel estimation for beyond diagonal RIS," *arXiv preprint arXiv:2412.02824*, 2024.

[13] H. Li, M. Nerini, S. Shen, and B. Clerckx, "Beyond diagonal reconfigurable intelligent surfaces in wideband OFDM communications: Circuit-based modeling and optimization," *IEEE Transactions on Wireless Communications*, vol. 24, no. 4, pp. 3623–3636, Apr. 2025.

[14] M. Samy, H. Al-Hraishawi *et al.*, "Beyond diagonal RIS-aided networks: Performance analysis and sectorization tradeoff," *IEEE Open Journal of the Communications Society*, pp. 1–1, 2024.

[15] T. Esmaeilbeig, K. V. Mishra, and M. Soltanalian, "Beyond diagonal RIS: Key to next-generation integrated sensing and communications?" *IEEE Signal Processing Letters*, vol. 32, pp. 216–220, 2025.

[16] K. Chen and Y. Mao, "Transmitter side beyond-diagonal RIS for mmwave integrated sensing and communications," in *2024 IEEE 25th International Workshop on Signal Processing Advances in Wireless Communications (SPAWC)*, 2024, pp. 951–955.

[17] W. U. Khan, C. K. Sheemar *et al.*, "Beyond diagonal IRS assisted ultra massive THz systems: A low resolution approach," in *2024 IEEE 35th International Symposium on Personal, Indoor and Mobile Radio Communications (PIMRC)*, 2024, pp. 1–5.

[18] A. Mahmood, T. X. Vu, S. Chatzinotas, and B. Ottersten, "Enhancing indoor and outdoor THz communications with beyond diagonal-IRS: Optimization and performance analysis," in *35th International Symposium on PIMRC*, 2024, pp. 1–6.

[19] W. U. Khan, E. Lagunas, A. Mahmood, M. Asif, M. Ahmed, and S. Chatzinotas, "Integration of beyond diagonal RIS and UAVs in 6G NTNs: Enhancing aerial connectivity," *IEEE Wireless Communications*, vol. 32, no. 3, pp. 56–63, June 2025.

[20] W. U. Khan, E. Lagunas, and S. Chatzinotas, "Transmissive beyond diagonal RIS-mounted LEO communication for NOMA IoT networks," *arXiv preprint arXiv:2501.02742*, 2025.

[21] J. A. Bondy and U. S. R. Murty, *Graph theory*. Springer Publishing Company, Incorporated, 2008.